New measurements of the $^{19}F(n, \gamma)^{20}F$ cross section and their implications for the stellar reaction rate

Ethan Uberseder,[1,2,*] Michael Heil,[1] Franz Käppeler,[1] Joachim Görres,[2] and Michael Wiescher[2]
[1]*Forschungszentrum Karlsruhe, Institut für Kernphysik, D-76021 Karlsruhe, Germany*
[2]*University of Notre Dame, Department of Physics, Notre Dame, Indiana 46556, USA*
(Received 2 October 2006; published 8 March 2007)

The puzzle concerning the nucleosynthetic origin of ^{19}F has been a topic of much interest in astrophysics. After the observation of an overabundance of ^{19}F in thermally pulsing asymptotic giant branch (AGB) stars, attention has been drawn to the He shell flash, characteristic of these stars, as a possible site of fluorine synthesis. As the He intershell of AGBs is also known to undergo periods of high neutron exposure, ^{19}F synthesized in this zone would be in danger of destruction by $^{19}F(n, \gamma)^{20}F$. The current recommended value of the Maxwellian averaged cross section (MACS) is uncertain by 20% in a temperature region corresponding to the He flash, which is insufficient for accurate stellar modeling. A measurement of the cross section has been performed at the Karlsruhe 3.7 MV Van de Graaff accelerator by cyclic activation of fluorine samples in a quasistellar neutron spectrum with a mean thermal energy of $kT = 25$ keV. The new MACS at $kT = 25$ keV is 44% lower and six times more accurate than reported previously.

DOI: 10.1103/PhysRevC.75.035801 PACS number(s): 26.20.+f, 25.40.Lw, 27.30.+t

I. INTRODUCTION

An extensive amount of research has been done concerning the stellar production of fluorine. Woosley *et al.* [1] proposed that ^{19}F is produced in type II supernovae via a neutrino process. Later Jorissen *et al.* [2] reported on an observational overabundance of ^{19}F in asymptotic giant branch (AGB) stars, strongly suggesting AGBs to be a significant site for fluorine production. A second article suggests a nucleosynthetic path operative during the thermal pulses characteristic of these stars [3]. During the radiative phase between thermal pulses, the $^{13}C(\alpha, n)^{16}O$ reaction, known to be the dominant neutron source for the main component of the *s* process [4], is operative. ^{14}N is abundant in the He intershell from the CNO ashes of the H burning phase and can utilize the liberated neutrons to produce ^{18}O through the reaction path $^{14}N(n, p)^{14}C(\alpha, \gamma)^{18}O$. In addition, ^{18}O is synthesized via $^{14}N(\alpha, \gamma)^{18}F(\beta^+\nu)^{18}O$. The protons resulting from the first reaction sequence contribute to an enhancement of ^{15}N in the helium intershell through $^{18}O(p, \alpha)^{15}N$, though the newly synthesized ^{15}N can act as a proton poison thus constraining further production. Furthermore, alpha capture can remove ^{18}O from the supply chain. A secondary source of ^{15}N can arise from proton capture on ^{14}N and subsequent β^+ decay at the base of the convective envelope during hot bottom burning [5]. Following the synthesis of ^{15}N, fluorine is produced via the $^{15}N(\alpha, \gamma)^{19}F$ reaction. The the rates of a large portion of these reactions have been studied, reviewed, and discussed recently (see Lugaro *et al.* [6]). During the He flash, fluorine is destroyed through the $^{19}F(\alpha, p)^{22}Ne$ and $^{19}F(n, \gamma)^{20}F$ reactions. Recent measurements have have investigated the contributions of low-energy resonances in $^{19}F(\alpha, p)^{22}Ne$ and have reduced the uncertainty in the reaction rate considerably [7]. The cross section of $^{19}F(n, \gamma)^{20}F$ at $kT = 30$ keV is given in Bao *et al.* [8] with an uncertainty of 20%. The aim of this work is to quantify the stellar neutron capture cross section of fluorine with a significant reduction in uncertainty.

In Sec. II, the experimental setup is described in detail. Section III reviews the method to extract a cross section from cyclic activation data. The results of the measurements are reported and discussed in an astrophysical context in Sec. IV, and a short summary follows in Sec. V.

II. EXPERIMENT

The activation technique is a well-known method to measure stellar neutron capture cross sections with high accuracy [9]. It is applicable when the produced nuclei are radioactive with characteristic particle or γ-ray emission. In the case of nuclei with short half-lives, the standard formulas can be adapted for use in a cyclic activation process [10]. Due to the half-life of ^{20}F, $t_{1/2} = 11$ s, the present series of measurements utilized this technique.

A. Samples

Various compounds were decided on for the production of the fluorine samples. Experimental runs were performed with SrF_2, NaF, and $(CF_2)_n$ disks, 6 and 10 mm in diameter, sandwiched between two gold foils of equally corresponding diameters. As the cross section of gold is precisely known for the experimental neutron distribution [11], the total neutron exposure could be accurately quantified. The samples were prepared from high-purity powdered material pressed into thin stable disks. The physical properties of the samples and gold foils are given in Table I.

B. Cyclic irradiation and counting

During a cyclic activation, the sample is irradiated for a time interval and then counted for an equal period with a HPGe detector. For these measurements, a pneumatic slide trans-

*Electronic address: Ethan.Uberseder.1@nd.edu

TABLE I. Physical properties of samples and Au foils.[a]

Sample	Diameter (mm)	Mass (mg)	F in sample (mg)	Au foil	
				Upstream (mg)	Downstream (mg)
$(CF_2)_n$-1	6	63.11	47.95	15.74	15.67
$(CF_2)_n$-2	10	161.05	122.37	46.30	44.58
SrF_2-1	10	165.42	50.04	46.39	46.30
NaF-1	10	129.54	58.61	43.26	44.52
NaF-2	10	184.41	83.44	43.79	43.16

[a]A conservative uncertainty of ± 0.05 mg has been assumed in all mass measurements.

ported the sample 50 cm from the irradiation to the detection position with a measured transfer time of $t_w = 0.80 \pm 0.05$ s. Although the samples were irradiated, the data acquisition system was gated to prevent the γ background originating in the neutron production target from being recorded. For the counting interval, a beamstop blocked the incident proton beam. The exchange system was automatically regulated via a control module. The irradiation and detection intervals were determined to be $t_b = t_m = 29.2 \pm 0.5$ s. Considering two additional transfer periods, the total time of one cycle equaled 60 ± 1 s.

The samples were exposed to quasistellar neutron spectra closely reproducing a Maxwell-Boltzmann distribution at $kT = 25$ keV [11] (see Fig. 1) corresponding to a temperature of $T_8 = 2.9$, very near to typical temperatures of the AGB He flash ($T_8 \approx 2.6$). The neutrons were produced via the ^{7}Li$(p, n)^7$Be reaction with an incident proton energy of 1911 keV, 30 keV above the reaction threshold. The incident proton beam was supplied by the Karlsruhe 3.7 MV Van de Graaff accelerator with an average beam current of 75μA. The beam energy was calibrated to the reaction threshold. At the specified proton energy neutrons are kinematically collimated to form a forward cone with an opening angle of 120°, and the sample was placed such that it fully intersected the neutron cone. A neutron monitor was placed 83 cm from the neutron production target at 0° to the beam axis. This monitor was used

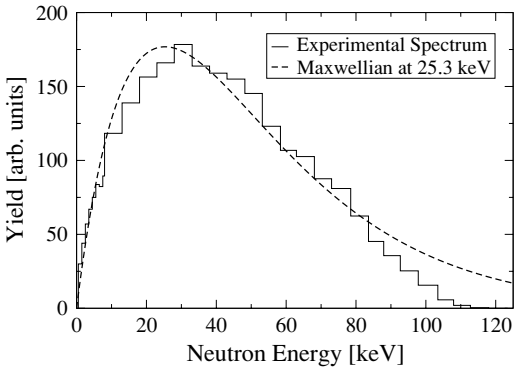

FIG. 1. Experimental yield of ^{7}Li$(p, n)^7$Be at $E_p = 1911$ (histogram) keV shown in comparison with an ideal Maxwell-Boltzmann distribution at $kT = 25$ keV.

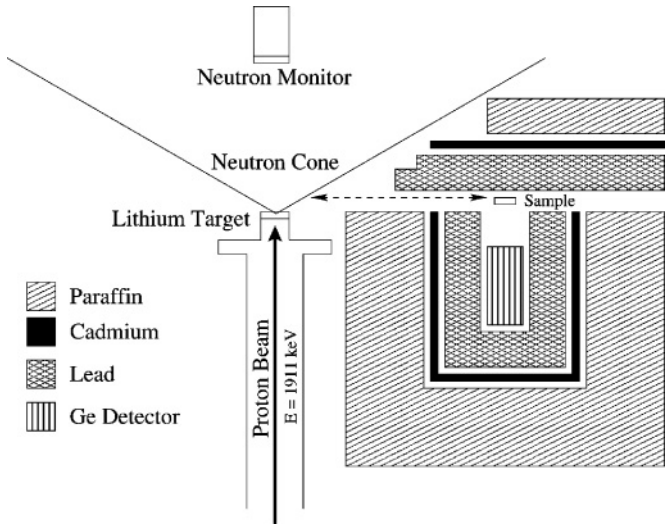

FIG. 2. Detector setup for the cyclic activation.

to record the neutron flux as a function of time, necessary to correct for decays of the product nuclei during irradiation.

The detector setup is shown in Fig. 2. An HPGe detector was positioned approximately 25 cm from the sample in the detection position. Such a large source-detector distance minimized the need for summing or extended-source corrections. The efficiency as a function of energy was determined to an uncertainty of 1.5% using calibrated radioactive sources, and Monte Carlo simulations were performed to correct for summing effects. A thick paraffin shield doped with lithium and boron enclosing a thin layer of Cd was used to reduce neutron-induced activity in the detector. Within this paraffin shield, and directly surrounding the detector crystal, 5 cm of lead reduced the γ background during the counting phase. Care was taken that the line of sight between the detector window and the sample was kept clear. For the analysis, the ^{20}F decay line at 1634 keV was chosen due to its high emission probability and can be seen appearing prominently above background in Fig. 3. With the longer half-life of

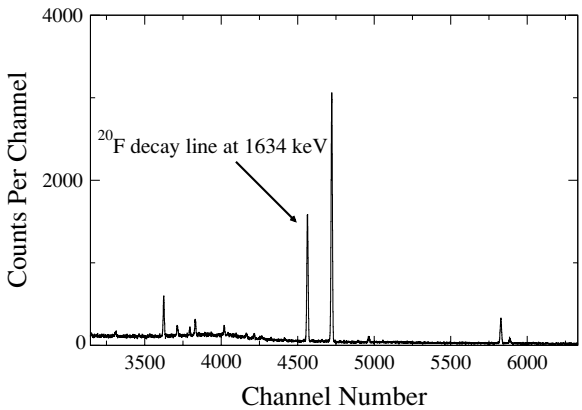

FIG. 3. Gamma spectrum showing the ^{20}F decay line. Other lines in the spectrum result from activated materials surrounding the detector, principally, the 1691 keV decay line from ^{124}Sb produced in the lead shield.

TABLE II. Properties related to γ-decay.

Nucleus	E_γ (keV)	$t_{1/2}$	ϵ_γ (%)	I_γ (%)
^{20}F	1634	11.163 ± 0.008[a] s	0.110 ± 0.002[b] 0.104 ± 0.002[c]	99.9995 ± 0.0[a]
^{198}Au	412	2.69517 ± 0.00021[d] d	0.224 ± 0.007	95.58 ± 0.12[d]

[a]Reference [12].
[b]Valid for $(CF_2)_n$ and SrF_2 samples.
[c]Valid for NaF samples.
[d]Reference [13].

^{198}Au, it was possible to count the induced gold activity following the cyclic activation process. The gold counts were accumulated in another HPGe detector located in a low background environment. The efficiency of this detector was accurately known to 1.5% for a reproduceable geometry. The individual gold foils were placed 76 mm from the detector window, and counts in the ^{198}Au decay line at 412 keV were accumulated. The quantities relating to the decay lines, needed in the analysis, are given in Table II.

III. ANALYSIS

The standard activation method is detailed by Beer and Käppeler [9]. The number of activated nuclei following irradiation is given by

$$A = \sigma N \Phi_T f_b, \tag{1}$$

where N is the number of sample nuclei per cm^2, $\Phi_T = \int \Phi(t)dt$ is the time integrated neutron flux, σ is the cross section in cm^2, and

$$f_b = \frac{\int_0^{t_b} \Phi(t) e^{-\lambda(t_b - t)} dt}{\int_0^{t_b} \Phi(t) dt}$$

is the correction factor for the decay of the product nuclei during irradiation. The number of counts registered in the detector after irradiation is

$$C = A \epsilon_\gamma K_\gamma I_\gamma e^{-\lambda t_w}(1 - e^{-\lambda t_m}). \tag{2}$$

Here, ϵ_γ is the detector efficiency, K_γ is the correction for γ-ray self-absorption in the sample, and I_γ is the emission probability of the decay line. K_γ can be evaluated analytically as

$$K_\gamma = \exp\left(\frac{-m_{\mathrm{Au}}^{\mathrm{front}} \mu_{\mathrm{Au}}}{\pi r^2}\right) \times \frac{\pi r^2}{m_s \mu_s}\left[1 - \exp\left(\frac{-m_s \mu_s}{\pi r^2}\right)\right].$$

The first portion of the equation corrects for the decay γs absorbed through the front gold foil and is necessary only when the sample is counted with the foil in place, whereas the latter is the correction for absorption in the sample averaged over the volume. The constants μ_{Au} and μ_s are the absorption coefficients for gold and the sample material, respectively, given at the γ energy of the investigated line. For the present analysis, these parameters were taken from Berger *et al.* [14]. The quantities $m_{\mathrm{Au}}^{\mathrm{front}}$ and m_s are the masses of the front gold foil and the sample, whereas r is the sample radius.

In the case of a cyclic activation, the counts registered per detection phase must also contain a correction for the activity remaining from previous irradiation phases, as represented in the following equation:

$$C_i = \sigma N \epsilon_\gamma K_\gamma I_\gamma e^{-\lambda t_w}(1 - e^{-\lambda t_m}) \sum_{k=1}^{i} \Phi_T^k f_b^k e^{-\lambda(i-k)t_c}.$$

In this equation, t_c is the duration of one cycle, and Φ_T^i and f_b^i are the time-integrated neutron fluxes and irradiation decay factors of cycle i, respectively. The sum of all counts accumulated in the detector over n cycles can then be represented by

$$\begin{aligned}\sum_{i=1}^{n} C_i &= \sigma N \epsilon_\gamma K_\gamma I_\gamma e^{-\lambda t_w}(1 - e^{-\lambda t_m}) \sum_{i=1}^{n}\sum_{k=1}^{i} \Phi_T^k f_b^k e^{-\lambda(i-k)t_c} \\ &= \frac{\sigma N \epsilon_\gamma K_\gamma I_\gamma e^{-\lambda t_w}(1 - e^{-\lambda t_m})}{1 - e^{-\lambda t_c}} \\ &\quad \times \sum_{i=1}^{n} \Phi_T^i f_b^i (1 - e^{-\lambda(n-i+1)t_c}).\end{aligned} \tag{3}$$

This equation should be used when the cycle time is long enough that significant changes in neutron flux are possible during each irradiation phase. If the irradiation phase is short in comparison to the variation in neutron flux, then the irradiation decay factor can be evaluated analytically as

$$f_b = \frac{1}{t_b}\int_0^{t_b} e^{-\lambda(t_b - t)} dt = \frac{1}{t_b \lambda}(1 - e^{-\lambda t_b}).$$

Thus the total counts expected from Eq. (3) becomes

$$\begin{aligned}\sum_{i=1}^{n} C_i &= \frac{\sigma N \epsilon_\gamma K_\gamma I_\gamma e^{-\lambda t_w}(1 - e^{-\lambda t_m})(1 - e^{-\lambda t_b})}{\lambda t_b (1 - e^{-\lambda t_c})} \\ &\quad \times \sum_{i=1}^{n} \Phi_T^i (1 - e^{-\lambda(n-i+1)t_c}) \\ &= \frac{\sigma N \epsilon_\gamma K_\gamma I_\gamma e^{-\lambda t_w}(1 - e^{-\lambda t_m})(1 - e^{-\lambda t_b})}{\lambda t_b (1 - e^{-\lambda t_c})} \\ &\quad \times \left(1 - f_c e^{-\lambda t_c}\right)\Phi_T,\end{aligned} \tag{4}$$

where

$$f_c = \frac{\sum_{i=1}^{n} \Phi_T^i e^{-\lambda(n-i)t_c}}{\sum_{i=1}^{n} \Phi_T^i}.$$

TABLE III. Experimental $^{19}F(n,\gamma)^{20}F$ cross section at $kT = 25$ keV.

Sample	σ_{exp} (mb)	Uncertainty	
		Sys. (%)	Stat. (%)
$(CF_2)_n$-1	3.46	3.37	1.27
$(CF_2)_n$-2	3.50	3.35	1.07
SrF_2-1	3.63	3.35	1.47
NaF-1	3.46	3.35	1.16
NaF-2	3.64	3.35	1.09
Average	3.54	3.4	0.6

This form of the equation is given in Beer *et al.* [10]. Again, Φ_T represents the time-integrated neutron flux over all cycles and is determined by the activity of the gold foils following irradiation. The time-integrated neutron flux per cycle can be evaluated further from the neutron history registered in the monitor. Considering the short irradiation time used in this series of measurements, Eq. (4) is well suited for the present analysis.

IV. RESULTS AND DISCUSSION

The experimental cross sections obtained during each run are given in Table III. Averaging over the five measurements yields an experimental cross section of $3.54 \pm {}^{0.12(sys.)}_{0.02(stat.)}$ mb. The contributions to the systematic uncertainty have been compiled in Table IV.

A. Maxwellian averaged cross section

Within a stellar interior, neutrons are thermalized and can be described by a Maxwell-Boltzmann distribution. For use in an astrophysical context, the experimental cross section must be given in terms of a Maxwellian averaged cross section (MACS). Mathematically, a MACS is defined by [8]

$$\langle\sigma\rangle_{kT} = \frac{\langle\sigma v\rangle}{v_T} = \frac{2}{\sqrt{\pi}} \frac{\int_0^\infty \sigma(E_n) E_n e^{-E_n/kT} dE_n}{\int_0^\infty E_n e^{-E_n/kT} dE_n}. \quad (5)$$

In this equation, $\sigma(E_n)$ is the cross section as a function of neutron energy, E_n is the neutron energy in the center-of-mass frame, and kT is the corresponding thermal energy of the distribution. Although the activation technique yields limited information about the energy dependence of the cross section, the laboratory neutron spectrum is tailored to closely reproduce a stellar distribution at $kT = 25$ keV. Center-of-mass corrections vary the experimental thermal energy slightly for lighter elements, and this effect was considered in the analysis. A rough approximation of the stellar MACS at $kT = 25$ keV can be made by the application of the normalization constant (i.e., $2/\sqrt{\pi} \times \sigma_{exp} = 3.99$ mb). As the laboratory distribution is truncated at $E_n = 106$ keV, a more careful determination of the true MACS at 25 keV took into account this and other subtle differences in the spectra. For this procedure, the energy-dependent cross section was obtained from an evaluated database [15–17]. Assuming an accuracy in the shape of the given energy dependence, the data were normalized to yield the measured value when averaged over the experimental distribution. Using Eq. (5), a true MACS was subsequently determined from the normalized data at the desired thermal energy. It should be noted that the energy dependence of the JEFF [15], ENDF/B [16], and JENDL [17] databases differ, though a maximum deviation of only 1.6% in the $kT = 25$ keV MACS value results from the analysis described above. In Table V, the results of this reduction have been calculated for these three energy-dependent cross sections and an average MACS at $kT = 25$ keV is shown. MACSs are also given for a range of thermal energies relevant to stellar nucleosynthesis and compared with the previous Bao *et al.* [8] values.

TABLE IV. Contributions to the total systematic cross section uncertainty.

Source	Au (%)	Sample (%)
Timing uncertainties and decay properties	<0.1	2.0
Au cross section	1.7	N/A
Number of nuclei	0.2	<0.1
γ-ray absorption	<0.1	<0.1
Detector peak efficiency	1.5	1.5
γ intensity	0.1	<0.1
Total uncertainty from Φ_T	N/A	2.3
Total systematic uncertainty		3.4

Considering the good agreement between a true Maxwell-Boltzmann distribution at $kT = 25$ keV and the experimental spectrum, it is assumed that the uncertainty in the extrapolation from the measured value to a true MACS is negligible. Therefore, the error given in Table V is the uncertainty of the measured value. It is important to mention that the method of normalizing a database cross section to reproduce a measured value yields accurate MACSs in the local energy region of the activation, but the extrapolations to further thermal energies are prone to increasing uncertainty. The results of this work clearly show a significantly reduced value of the MACSs with respect to those given in Bao *et al.* [8]. The previously known neutron capture data concerning fluorine is mostly derived from the work of Allen *et al.* [18], Macklin and Winters [19], Gabbard *et al.* [20], and Nyström *et al.* [21]. These older time-of-flight measurements have been seen to differ significantly from more recent activations, primarily as a result of insufficient corrections for scattered neutrons. Furthermore, this new measurement reduces the uncertainty of the MACS in the region around $kT = 25$ keV by approximately a factor of 6 due to the sensitivity and precision of the activation technique. A more recent publication by Lee *et al.* [22] cites new radiation widths for the 27, 49, and 97 keV resonances in ^{20}F. Based on these parameters, we estimate a 30% reduction in the $kT = 25$ keV MACS with respect to the Bao *et al.* [8] value. Another activation measurement using the $kT = 25$ keV thermal neutron spectrum quotes an experimental value of 3.77 ± 0.11 mb [23], though only the statistical error is given with no mention of systematics.

TABLE V. Maxwellian averaged neutron capture cross sections of ^{19}F.

	MACS (mb)										
Thermal energy (keV)	5	10	15	20	25	30	40	50	60	80	100
This work	1.2	4.1	4.5	4.2	**3.7 ± 0.1**	3.2	2.5	2.0	1.7	1.2	1.0
Bao *et al*. [8]	2.0	6.7	7.8	7.4	6.6	5.8 ± 1.2	4.6	3.8	3.2	2.5	2.2

B. Implications for ^{19}F production

A significant reduction in the MACS of ^{19}F$(n, \gamma)^{20}$F at temperatures relevant to the He flash in AGB stars may indicate an increased survival of fluorine during this phase of AGB evolution. This, however, depends also on on the strength of the competing ^{19}F(α, p) depletion reaction in the He flash. This reaction has been measured recently and the results are being prepared for publication [7]. Following the He flash, the nucleosynthetic products of the He intershell are brought to the surface of the star in what is known as the third dredge-up (TDU). Here, the convective tongue of the envelope extends into the He intershell, and the produced nuclei are mixed upward. Fluorine can again be destroyed by proton induced reactions in the envelope, mainly through the ^{19}F$(p, \alpha)^{16}$O reaction [6]. A recent measurement by Couture [24] has reduced the stellar reaction rate of ^{19}F$(p, \gamma)^{20}$Ne by a factor of 4. This experiment also produced data concerning the ^{19}F$(p, \alpha\gamma)^{16}$O channel, and a complete R-matrix analysis considering both reaction pathways is currently underway. The systematic reduction of these destruction reaction rates would significantly increase the AGB surface abundance of fluorine. Detailed stellar model calculations are presently in preparation, taking into account all recent experimental results, that will quantify the impact of the present cross section on the AGB surface abundances.

V. SUMMARY

Measurements of the ^{19}F$(n, \gamma)^{20}$F cross section at $kT =$ 25 keV have been performed at the Karlsruhe 3.7 MV Van de Graaff accelerator. The value of $\langle\sigma\rangle_{kT=25\text{keV}} = 3.69 \pm {}^{0.12(\text{sys.})}_{0.02(\text{stat.})}$ mb recommended by the present work is significantly lower than what is given in the literature [8]. This work also lowers the uncertainty in the cross section by a factor of 6 with respect to Bao *et al*. [8]. Such a reduction in the cross section of fluorine might result in a notably increased survival of ^{19}F through the duration of the He flash in AGB stars. This, however, depends sensitively on the strength of the competing depletion reactions ^{19}F$(\alpha, p)^{22}$Ne and ^{19}F$(p, \alpha)^{16}$O. Barring significant destruction of fluorine in the envelope, such a contribution could further support the importance of AGB stars in fluorine nucleosynthesis.

ACKNOWLEDGMENTS

The authors are thankful to D. Roller, E.-P. Knaetsch, W. Seith, and the entire Van de Graaff staff for their support during the measurements. This work was supported by the Joint Institute for Nuclear Astrophysics (JINA), University of Notre Dame, Notre Dame, IN through NSF grants PHY02-16783 and PHYO4-57120.

[1] S. Woosley, D. Hartmann, R. Hoffman, and W. Haxton, Astrophys. J. **356**, 272 (1990).
[2] A. Jorissen, V. Smith, and D. Lambert, Astron. Astrophys. **261**, 164 (1992).
[3] M. Forestini, S. Goriely, A. Jorissen, and M. Arnould, Astron. Astrophys. **261**, 157 (1992).
[4] F. Käppeler, Prog. Part. Nucl. Phys. **43**, 419 (1999).
[5] N. Mowlavi, A. Jorissen, and M. Arnould, Astron. Astrophys. **334**, 153 (1998).
[6] M. Lugaro, C. Ugalde, A. Karakas, J. Görres, M. Wiescher, J. Lattanzio, and R. Cannon, Astrophys. J. **615**, 934 (2004).
[7] C. Ugalde, R. Azuma, A. Couture, J. Görres, H. Lee, E. Stech, W. Tan, and M. Wiescher, Phys. Rev. C, to be submitted (2007).
[8] Z. Bao, H. Beer, F. Käppeler, F. Voss, K. Wisshak, and T. Rauscher, At. Data Nucl. Data Tables **76**, 70 (2000).
[9] H. Beer and F. Käppeler, Phys. Rev. C **21**, 534 (1980).
[10] H. Beer, G. Rupp, G. Walter, F. Voss, and F. Käppeler, Nucl. Instrum. Methods A **337**, 492 (1994).
[11] W. Ratynski and F. Käppeler, Phys. Rev. C **37**, 595 (1988).
[12] D. Tilley, C. Cheves, J. Kelley, S. Raman, and H. Weller, Nucl. Phys. **A636**, 249 (1998).
[13] Z. Chunmei, Nucl. Data Sheets **95**, 59 (2002).
[14] M. Berger, J. Hubbell, S. Seltzer, J. Chang, J. Coursey, R. Sukumar, and D. Zucker, Xcom: Photon Cross Section Database, http://physics.nist.gov/PhysRefData/Xcom/Text/XCOM.html.
[15] A. J. Koning, O. Bersillon, R. A. Forrest, R. Jacqmin, M. A. Kellett, A. Nouri, and P. Rullhusen, in *Proceedings of the International Conference on Nuclear Data for Science and Technology, Santa Fe, 2004*, p. 177.
[16] M. B. Chadwick, P. Oblozinsky, and M. Herman *et al*., Nucl. Data Sheets **107**, 2931 (2006).
[17] K. Shibata *et al*., J. Nucl. Sci. Technol. **39**, 1125 (2002).
[18] B. Allen, D. Cohen, and F. Company, J. Phys. G: Nucl. Part. Phys. **6**, 1173 (1980).
[19] R. Macklin and R. Winters, Phys. Rev. C **7**, 1766 (1973).
[20] F. Gabbard, R. H. Davis, and T. Bonnor, Phys. Rev. **114**, 201 (1959).

[21] G. Nyström, B. Lundberg, and I. Bergqvist, Phys. Scr. **4**, 95 (1971).
[22] S. Y. Lee, J. Hori, and M. Igashira, J. Nucl. Sci. Technol. **36**, 719 (1999).
[23] P. Mohr, H. Oberhummer, and H. Beer, in *Proceedings of the 9th International Symposium on Capture Gamma-Ray Spectroscopy and Related Topics*, edited by G. Molnár, T. Belgya, and Z. Révay (Springer, Budapest, 1997), vol. 1, p. 428.
[24] A. Couture, Ph.D. thesis, University of Notre Dame (2005).